Detecting nanoscale contamination in semiconductor fabrication using through-focus scanning optical microscopy

Min-Ho Rim[1a)], Emil Agocs[2], Ronald Dixson, Prem Kavuri,
András E. Vladár and Ravi Kiran Attota

Microsystems and Nanotechnology Division, PML, NIST, Gaithersburg, MD 20899, USA
[1]SAMSUNG Electronics Co. Ltd. 1, Samsungjeonja-ro, Hwaseong-si, Gyeonggi-do 18448, Republic of Korea
[2]Current address: Institute for Technical Physics and Materials Science, Centre for Energy Research, Hungarian Academy of Sciences, Konkoly-Thege Rd. 29-33, 1121 Budapest, Hungary

[a)]Electronic mail: minho.rim@samsung.com

This paper reports high-throughput, light-based, through-focus scanning optical microscopy (TSOM) for detecting industrially relevant sub-50 nm tall nanoscale contaminants. Measurement parameter optimization to maximize the TSOM signal using optical simulations made it possible to detect the nanoscale contaminants. Atomic force and scanning electron microscopies were used as reference methods for comparison.

I. INTRODUCTION

Detection of nanoscale contaminants, including individual or aggregates of nanoparticles, is a challenge for the current semiconductor industry as it could severely impact the yield of the fabrication process [1]. With the ever-shrinking design-rule, increasingly smaller size contaminants must be detected, and their numbers kept below an acceptable level. Due to the very weak signals generated by small contaminants, conventional optical microscopes in direct imaging mode have reached their limits.

Several imaging techniques have been developed to enhance the resolution and sensitivity of light-based techniques for nano-scale size particle detection [2-5]. Many of them use fluorescence methods requiring nanoparticles to be fluorescent, which is generally not conducive in the semiconductor production. Hence it is beneficial to have label-free detection methods of nano-scale contaminants or particles for semiconductor industry applications. In addition, methods having high-throughput and low cost are a plus. Interferometric scattering microscopy (iSCAT) [3,4] is one such a method for nano-scale target detection that is label-free and has a high-throughput. iSCAT primarily relies on subtracting two optical images (i.e. differential-imaging), one with the nano-scale target and the other without it. Similar differential-imaging procedures have been used by through-focus scanning optical (TSOM) [6-13] and scatterfield microscopy [14] to detect nanoscale defects. However, TSOM and scatterfield microscopy use many through-focus differential images instead of a single differential image used by iSCAT. The additional optical information analyzed by TSOM and scatterfield microscopy methods provide them with an added benefit of not only detecting nano-scale targets, but also measure and analyze them. Here we use primarily TSOM to detect nano-scale contaminations relevant for semiconductor industry. In this case TSOM uses

differential imaging to remove the optical background noise.

TSOM is not an image resolution enhancement method, rather it takes advantage of acquiring more information than of a single, in-focus image and through this it achieves sub-nanometer measurement resolution [6,8]. TSOM uses a set of through-focus optical images for dimensional analysis. Due to its high sensitivity and ease of use, TSOM has been used for three-dimensional shape investigation of many types of targets with sizes ranging from smaller than 10 nm to larger than 100 µm, and several applications , including nanoparticle size determination [15]. A major advantage is the ability to use ubiquitous optical microscopes for TSOM measurements making it widely applicable.

Through-focus optical images of nanoparticles or bacteria produce images similar to an Airy disc [16-18], with unique variations (or diffraction patterns) depending on focus positions. Using this characteristic, tracking of nanoparticles and bacteria was performed [16]. The optical signal strength of these through-focus diffraction patterns, due to high-coherence illumination (low illumination numerical aperture), is significantly stronger compared to conventional optical imaging. Through-focus images can be assembled to produce TSOM images, which can be used to both track, and determine the size of nanoparticles. TSOM can be used to measure the size of nanoparticles [15], or alternatively to determine the number of polystyrene nanoparticles in a cluster [19].

The goal of this work is to evaluate the suitability of TSOM as a low-cost and a high-throughput method for detection of nanoscale contamination encountered in a typical semiconductor fabrication process. Si or SiO_2 are the most probable components of the contamination [1]. For this reason, silica (SiO_2) nanoparticles have been initially studied in the present work as a realistic model system. Even though general optimization of TSOM optical parameters was discussed previously [20,21], optimization specifically for silica nanoparticles has not yet been reported. Here we initially present optimization of measurement parameters specifically for silica nanoparticle detection, followed by application of TSOM for nanoparticle detection.

II. EXPERIMENTS

Two types of targets have been studied using TSOM, atomic force microscope (AFM), and critical-dimension scanning electron microscopy (CD-SEM). They were (i) commercially-available amine-terminated monodispersed silica nanoparticles (5% concentration in deionized water) with a nominal diameter of 80 nm (coefficient of variation of <10 %) on a Si substrate for the optimization experiment, and (ii) a contaminated wafer obtained from a typical industrial production environment.

A commercially available optical simulation software program that solves Maxwell's equations using finite-difference time-domain was used to determine the optimized parameters for measurements [22]. Silica nanoparticles of 80 nm diameter on Si substrate were used for this task. The native thin-film silica formed was ignored in this simulation. Illumination wavelength (λ), and illumination numerical aperture (INA) parameters were optimized to achieve practically the best possible signal for the TSOM analysis (more details on this process can be found in the section describing optimization).

Easily identifiable fiducial marks were initially created on an optically smooth Si substrate. The Si substrate was then cleaned using a solution of NH_4OH (30%), H_2O_2 (30%) and deionized (DI) water mixed at a ratio of 1:1:5, respectively, at 90°C for 20 min. Following this, the Si substrate was rinsed four times with DI water and was dried using a clean, dry nitrogen gas jet. The Si substrate was then functionalized to make the nanoparticles adhere to the surface.

The silica nanoparticles were then dropped at two dilutions (the original dilution of 5 %, and a dilution of 1 %) onto the prepared substrate to create different agglomerates of the nanoparticles. To prevent excessive agglomerations and to avoid too dense particle distributions, the substrate was immediately rinsed with DI water, followed by gentle blow-drying with clean, dry nitrogen gas. Both dilutions produced different agglomerates, but at different concentrations. However, the final selection of dimer, trimer and tetramer was made mainly by the SEM observation.

For these experiments, a conventional, research-grade optical microscope described in Refs. 23 and 24 was used. Bright-field optical images were acquired using a 50X magnification objective, with illumination (INA) and collection (CNA) numerical apertures of 0.13 and 0.95, respectively. Illumination wavelengths of 405 nm, 520 nm and 633 nm were used for optimization. Z-axis (focus axis) was controlled by a stepper motor with a minimum step size of 10 nm. Through-focus data were collected at a step size of 100 nm. Each image frame was collected using a 1.4 - million-pixel CMOS sensor with a dynamic range of 1:2500 at 12.5 MHz, and 14-bit gray level. The image normalization procedure reported in Refs. 21 and 25, and the software developed in-house to analyze the TSOM images were used. The signal strength of the nanoparticles was evaluated using optical intensity range (OIR), defined as the absolute difference between the maximum and the minimum optical intensity in a given TSOM image and multiplied by 100 [8]. Prior research has shown that the nanoparticle optical volume (size and/or number) correlates well with the OIR values [15,19].

Reference metrology of the nanoparticles was done using a commercially-available, CD-SEM [26], and well characterized and calibrated CD-AFM [27]. The CD-SEM was operated with electron landing energy and probe current of 5.0 keV and 43 pA, respectively.

III. RESULTS AND DISCUSSION

The AFM image (Fig. 1) shows relatively large contaminants with peak heights of 72 nm and 75 nm, which appear to be agglomerates. It is not difficult to detect these large objects with optical microscopes. However, detecting the smaller contaminants (e.g. in the rectangle) with optical microscopes is difficult. In this paper we study detectability of these relatively smaller contaminants with optimized TSOM.

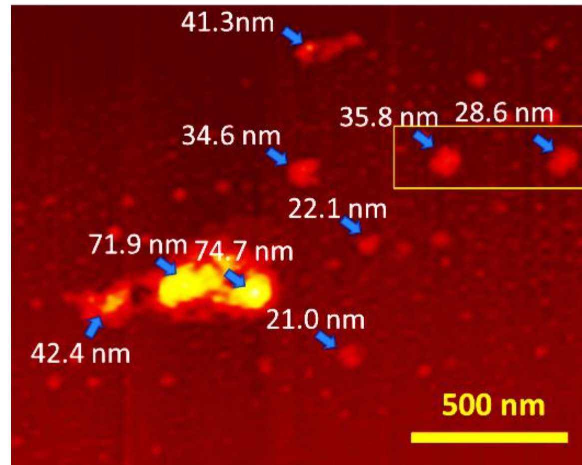

FIG. 1. A typical AFM image of the contaminated area on the wafer. The indicated numbers are the measured peak heights of the contaminants.

A. TSOM Optimization using simulations

The first task is to determine the parameters (λ and INA) producing the optimal optical signal of the TSOM images under the measurement conditions used here. The effects of λ and INA on TSOM images and their OIR values are shown in Fig. 2. It also shows the typical pattern produced by TSOM process with λ and INA. Under the current simulation conditions, it can be observed that decreasing either λ or INA increases the OIR. These results agree with the literature [21,28]. Summary plots of the OIR with λ and INA are shown in Figs. 2(f) and 2(g), respectively, clearly indicating this trend.

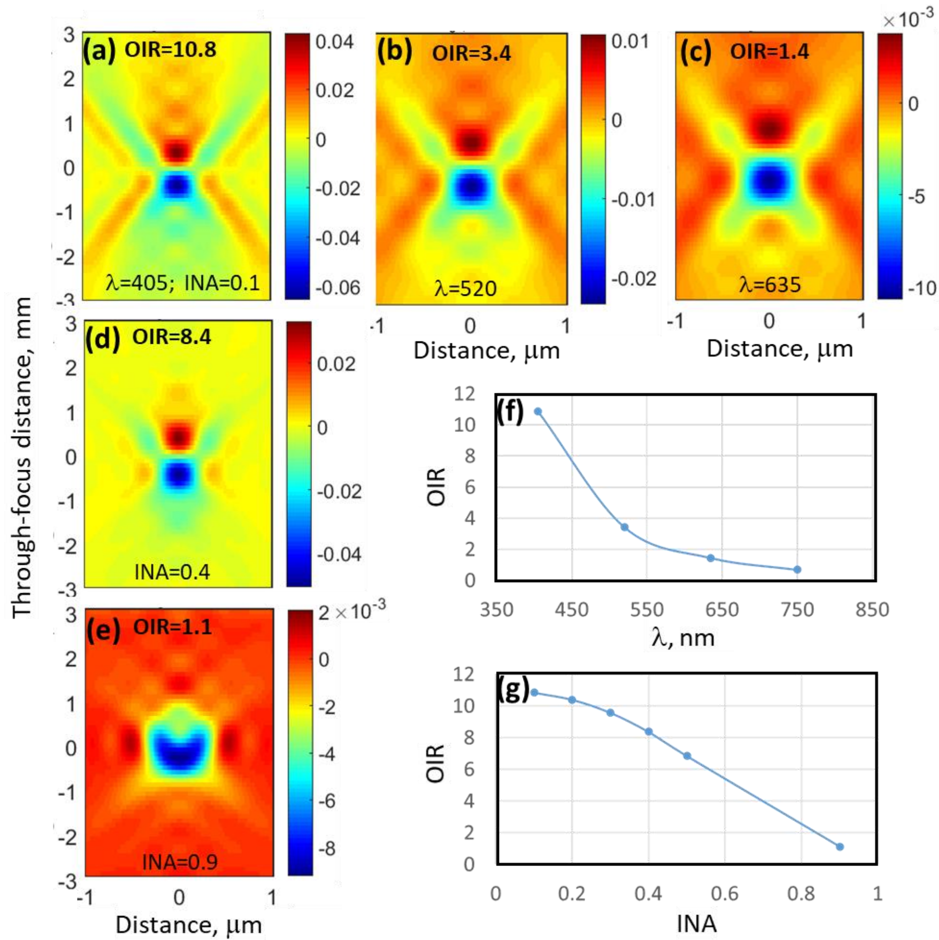

FIG. 2. Optimization of λ and INA for 80 nm diameter silica nanoparticles on Si substrate using optical simulations. (a), (b) and (c) TSOM images with variable λ, as indicated in the figures, at 0.1 INA. (a), (d) and (e) TSOM images with variable INA, as indicated in the figures, at a λ of 405 nm. Spline fitted plots to the OIR data are shown as a function of (f) λ, and (g) INA. Collection numerical aperture used was 0.95.

Even though the simulations indicate increased OIR with decreasing λ and INA, these parameters cannot be chosen below a certain level due to practical limitations. For example, in the microscope used the lowest λ available was 405 nm. Hence a λ of 405 nm was selected. Decreasing INA reduces the amount of light irradiating the sample. This in turn reduces the light collected by the camera resulting in a noisy optical image, below a certain intensity. The optical image intensity can be increased either by increasing the light source intensity or by increasing the camera exposure time. However, the light source intensity cannot be increased beyond the maximum brightness available, and the longer camera exposure time beyond a certain level can create other unwanted problems. Therefore, for the 50-times magnification objective, the lowest INA where satisfactory optical signal strength can be achieved was 0.13, with an optimized camera exposure time of 200 ms. For this reason, an INA of 0.13 and a λ of 405 nm were selected for the measurements.

B. Testing on silica nanoparticles

With the optimized parameters selected, through-focus optical data were collected for monomer, dimer and tetramer agglomerate silica nanoparticles. Through-focus optical images presented in Fig. 3(a) from one of the sets show typical variations in the optical images with focus position. A typical TSOM image extracted from one such set of through-focus optical image data is presented in Fig. 3(b). The red and blue areas shown there correspond to high and low detected intensity, respectively.

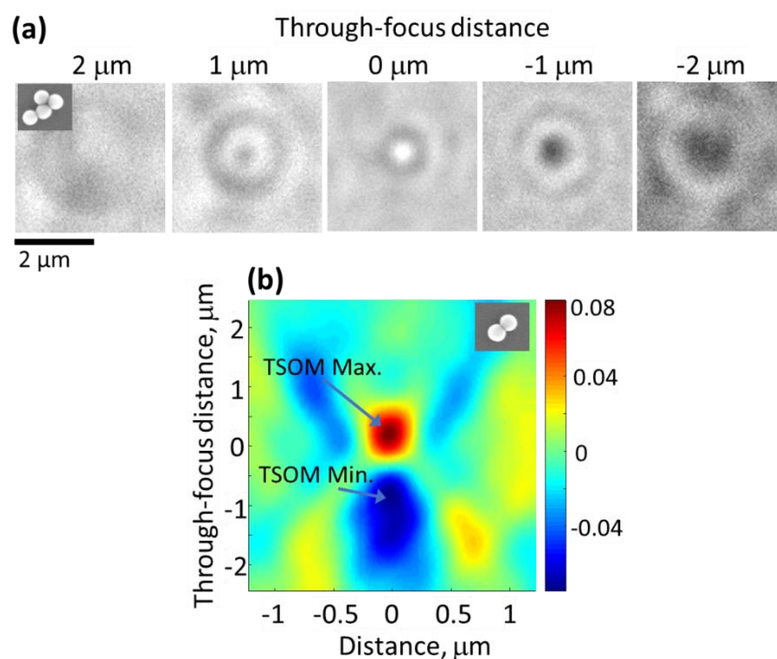

FIG. 3. (a) Typical optical images at various focus values. This set of 5 images was acquired using a tetramer silica nanoparticle agglomerate shown in the inset. (b) A typical constructed TSOM image from through-focus optical images. This TSOM image was constructed using a dimer nanoparticle agglomerate shown in the inset. The images shown in the insets were obtained using SEM. The nominal diameter of the silica nanoparticles is 80 nm.

An important goal of this work is to explore the feasibility of optical measurements with improved detectability of small contaminants. In Fig.2 we demonstrated how optimizing the optical parameters can increase the optical signal strength (i.e., OIR). OIR and the contrast for optical images as defined by the focus-metric in Ref. 29 are related. In general, increased focus-metric also increases OIR. Here we show how plotting the optical intensity profiles in the form of TSOM images increases the overall optical signal strength. To demonstrate this first the contrast (as evaluated using the focus-metric) for each through-focus optical image was plotted as a function of the focus position (Fig. 4(a)). Conventionally, the focus position where the highest contrast occurs is considered the best-focus optical image. For the tetramer, the highest contrast

value is about 38 A.U. The same through-focus data were then plotted in the form of TSOM images and the contrast values for them were evaluated in the similar way. The peak contrast values from Fig. 4(a) are compared with the contrast values evaluated from the three TSOM images as shown in Fig. 4(b). The contrasts from the TSOM images are consistently and substantially higher than the optical images. This shows that simply plotting the through-focus optical data in the form of a TSOM image increases the signal strength, and hence the signal-to-noise ratio, as noise level is nearly the same. This in turn enhances detectability.

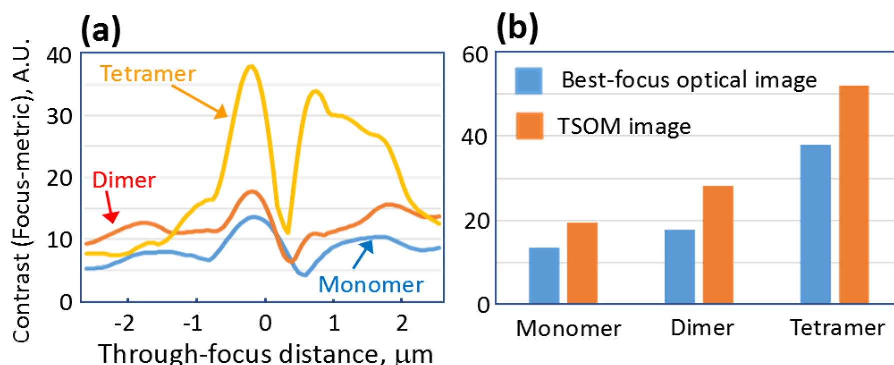

FIG. 4. (a) Typical contrast obtained from the through-focus optical images, and (b) Contrast comparison between the optical and the TSOM images for the monomer, dimer and tetramer agglomerates.

The two optimization methods presented so far significantly improved optical signal of nanoparticles. Conventionally, high INA is generally preferred to improve optical resolution [30]. However, in this work we have shown that using lower INA significantly enhanced the optical signal (Fig. 2(g)), albeit with a lower image resolution, which is not a constraint for the TSOM method described here. Secondly, shorter λ increased optical signal (Fig. 2(f)). In addition to these, through-focus optical data plotted in the form of a TSOM image enhanced signal strength and hence signal-to-noise ratio compared to the one best-focus optical image (Fig. 4(b)). In the following sections we make use of these three improved conditions to detect the nanoscale contamination.

C. Analysis of the realistic contaminants with TSOM

From the typical industrial contamination wafer, we selected two contaminants as indicated by the rectangle in Fig.1. Sometimes these contaminants are also referred to as defects. AFM images of these two contaminants are shown in Figs. 5(a1) and 5(a2) with measured peak heights of about 28.6 nm and 35.8 nm, respectively. SEM images of the same contaminants are presented in Figs. 5(b1) and 5(b2), respectively. The SEM images indicate that these are agglomerates forming nearly circular areas. The largest measured diameters are about 168 nm and 131 nm, respectively. Conventional optical images of the same contaminants showed weak signals indicating that it may not be possible to detect them.

The same contaminants were then analyzed using TSOM with parameters optimized to enhance the signal. The resulting TSOM images presented in Figs. 5(c1) and 5(c2) show strong signals demonstrating that these nanoscale contaminants can be identified using the TSOM optical method. In a previous publication it was shown that the noise floor of a TSOM image has an OIR value of about one [31]. The OIR values of the two contaminants (19.7 and 28.3, respectively) are significantly above this noise level making them easily identifiable. The results presented so far strongly indicate that the TSOM optical method is more effective in detecting nanoscale contaminants than the conventional bright-field optical microscopes.

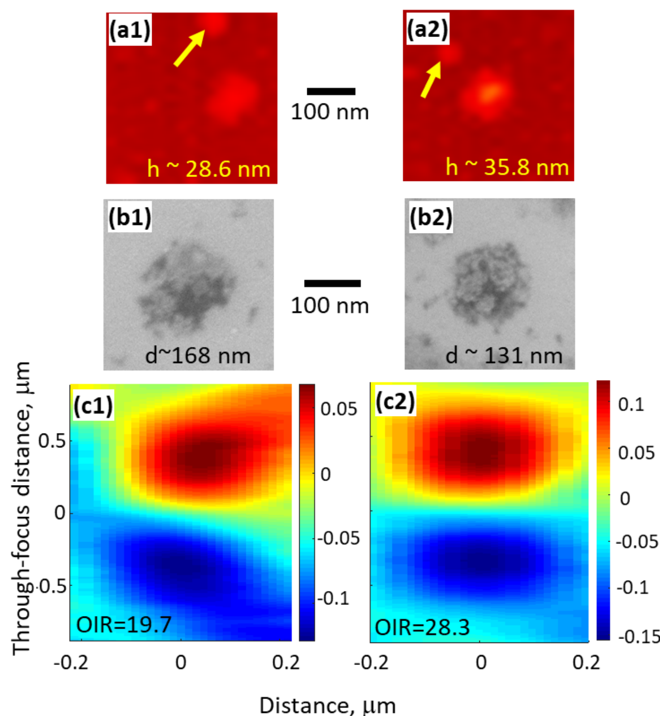

If two or more contaminants are located closer than half the illumination wavelength (for example see arrow marks in Figs.(a1) and (a2)), optical signals from them would interfere significantly. Closer the particles, higher the optical interference. Optical signals from such close contaminants would merge making them look like a single contaminant. Under such a condition it is hard to identify them as individual particles in the TSOM image. This is a disadvantage of optical methods, including the TSOM method. Such an interference some time can also distort the TSOM image shape, as can be seen in Fig. 5(c1).

With TSOM measurements, depending on the type of optical configuration selected, the data acquisition for a set of through-focus optical images can advantageously be as fast as acquiring a single optical image [32]. In addition, several contaminants present in a field-of-view can all be analyzed simultaneously, further improving the throughput. This high-throughput capability combined with the low cost of being an optical tool makes TSOM attractive for industrial contamination detection and analysis.

IV. CONCLUSIONS

We have presented an analysis of using TSOM for detecting nanoscale contamination typically encountered during semiconductor fabrication. Optimization of the measurement parameters and the use of through-focus optical data in the form of a TSOM image enhanced the optical signal significantly and enabled detection of nanoscale contamination. These benefits are paving the way for using low-cost and high-throughput TSOM for industrial high-volume manufacturing applications.

ACKNOWLEDGEMENTS

Dr. Rim would like to thank SAMSUNG Electronics Co., Ltd., for funding his one-year fellowship at NIST.

1. K. Reinhardt, Handbook of silicon wafer cleaning technology, 3rd edition. ed. (Elsevier, Waltham, MA, 2018).
2. P. Montgomery, A. Leong-Hoï, F. Anstotz, H. Liu, B. Simon, M. Debailleul, and O. Haeberlé, Proc. SPIE, 9890, 98900G (2016).
3. J. Ortega-Arroyo and P. Kukura, Phys. Chem. Chem. Phys .14, 15625-15636 (2012).
4. S. Spindler, J. Ehrig, K. Konig, T. Nowak, M. Piliarik, H. E. Stein, R. W. Taylor, E. Garanger, S. Lecommandoux, I. D. Alves, and V. Sandoghdar, J. Phys. D: Appl. Phys. 49, 274002 (2016).
5. V. Jacobsen, P. Stoller, C. Brunner, V. Vogel, and V. Sandoghdar, Opt. Express 14, 405 (2006).
6. R. Attota, B. Bunday, and V. Vartanian, Appl. Phys. Lett. 102, 222107 (2013).
7. R. Attota, R. Silver, and B. M. Barnes, Proc. SPIE 6922, 69220E (2008).
8. R. Attota and R. G. Dixson, Appl. Phys. Lett. 105, 043101 (2014).
9. R. Attota, R. G. Dixson, J. A. Kramar, J. E. Potzick, A. E. Vladar, B. Bunday, E. Novak, and A. Rudack, Proc. SPIE 7971, 79710T (2011).
10. M. Symeonidis, R. N. S. Suryadharma, R. Grillo, A. Vetter, C. Rockstuhl, T. Bürgi, and T. Scharf, Opt. Express 27, 20990 (2019).
11. Y. Qu, J. Hao, and R. Peng, Opt. Express 27, 33978 (2019).
12. S.W. Park, G. Park, Y. Kim, J. H. Cho, J. Lee, and H. Kim, Opt. Express 26, 11649 (2018).
13. M. Ryabko, S. Koptyaev, A. Shcherbakov, A. Lantsov, and S. Y. Oh, Opt. Express 22, 14958 (2014).
14. B. M. Barnes, Y. J. Sohn, F. Goasmat, H. Zhou, R. M. Silver, and A. Arceo, Proc. SPIE 8324, 83240F (2012).
15. R. Attota, P. P. Kavuri, H. Kang, R. Kasica, and L. Chen, Appl. Phys. Lett .105, 163105 (2014).
16. K. M. Taute, S. Gude, S. J. Tans, and T. S. Shimizu, Nat. Comm. 6, 8776 (2015).
17. E. A. Patterson and M. P. Whelan, Nanotechnology 19 , 105502 (2008).
18. J. M. Gineste, P. Macko, E. A. Patterson, and M. P. Whelan, J. of Microscopy 243, 172 (2011).
19. H. Kang, R. Attota, V. Tondare, A. E. Vladar, and P. Kavuri, Appl. Phys. Lett. 107, 103106 (2015).
20. R. Attota and J. Kramar, Proc. SPIE 9778, 977811 (2016).
21. R. K. Attota and H. Kang, Opt. Express 24, 14915 (2016).
22. T. V. Pistor, "Electromagnetic Simulation and Modeling with Applications in Lithography," Ph.D. Thesis, Univ. California, Berkeley, 2001.
23. R. K. Attota, Opt. Express 24, 22616 (2016).
24. E. Agocs and R.K. Attota, Sci. Rep-UK , 8, 4782 (2018).
25. R. Attota, Opt. Lett., 41, 745 (2016).
26. M. T. Postek, A. E. Vladár, and K. P. Purushotham, Scanning 36, 347 (2014).
27. R. Dixson, N. G. Orji, C. D. McGray, J. Bonevich, and J. Geist, J. Micro-Nanolith Mem. 11, 011006 (2012).
28. E. A. Patterson and M. P. Whelan, Small 4, 1703 (2008).
29. R. Attota, R. M. Silver, and J. Potzick, Proc. SPIE, 6289, 62890Q (2006).
30. M. Abramowitz and M. W. Davidson, Numerical Aperture and Resolution, https://micro.magnet.fsu.edu/primer/anatomy/numaperture.html, (2018).
31. A. Arceo, B. Bunday, V. Vartanian, and R. Attota, Proc. SPIE, 8324, 83240E (2012).
32. R. Attota, J. Biomed Opt., 23, 19100 (2018).